ROTORDYNAMIC PERFORMANCE OF GAS FOIL BEARINGS

Alejandro C. Martinez, UG REU Student
Tae Ho Kim, Research Assistant
Chad Jarrett, Research Assistant
Dr. Luis San Andrés, Principal Investigator

Introduction

Gas Foil Bearings (GFBs) are a proven alternative to rolling element bearings for high speed applications. GFBs eliminate lubrication, have no DN limit, and withstand high temperature operation. However, GFBs show little damping and have limited load capacity.

The research objective is to measure and analyze effect of (externally applied) static load on the dynamic forced performance of rotor supported on GFBs.

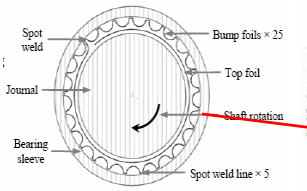

Fig 1. Schematic view of gas foil bearing used in tests.

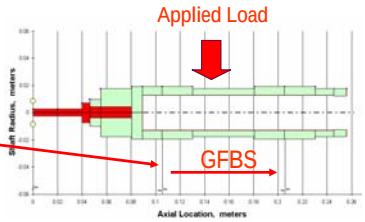

Fig 2. Structural FE model of test rotor

Test Apparatus

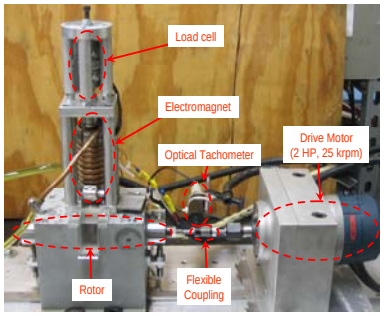

Fig. 3. Photograph of GFB test rig

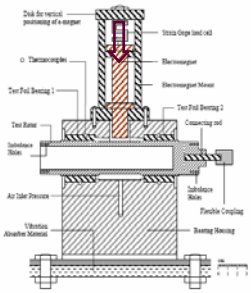

Fig. 4. Cross section view of GFB test rig

2.2 lb hollow rotor supported on a pair of GFBs driven by AC router motor. An electromagnet on the bearing housing applies a no-contacting load on the rotor. Voltage changes vary the magnitude of applied static load. A load cell measures the force and eddy current sensors record the horizontal and vertical displacement at both ends of the test rotor.

Test Results

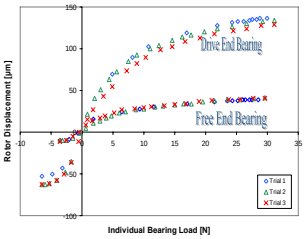

Fig. 5: Static displacement of free and drive end bearings with increasing load. No coupling attached

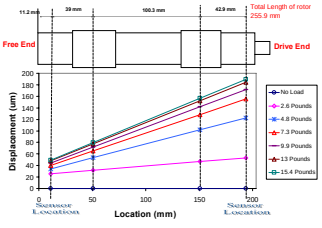

Fig. 6: Effect of increasing load on rotor end displacements. No coupling attached.

Figures 5 and 6 show the static load results with no coupling attached. Larger rotor displacement at the drive end are due to the larger clearance on the drive end bearing (softer bearing). The data shows that static bearing deflections are nonlinear, best described by a third order polynomial. Figure 7 depicts the effect of the coupling on rotor deflections. Figure 8 demonstrates mechanical element hysteresis under cyclic loading conditions and due to dry-friction.

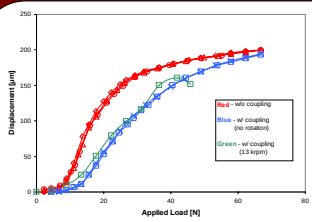

Fig. 7. Comparison of rotor end static displacements with and without coupling attached. Additional coupling stiffness reduces displacements. This effect remains with shaft rotation.

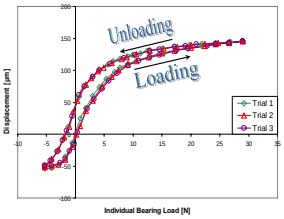

Fig. 8: Drive end rotor displacement vs applied load for several cycles of loading and unloading. The consistently higher displacements during unloading evidences hysteresis.

Rotor speed coast down tests from 13 krpm conducted next. Figures 9 thru 13 show selected test dynamic results. Increasing static loads reduce drastically rotor coast down time and eliminate 2X synchronous vibrations. Rotor motion with largest orbit amplitude shows passage thru critical speed. Increasing the static load reduces vibration amplitude at critical speed but does not affect its location.

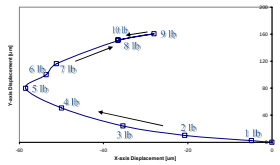

Fig. 9. Displacement of rotor center at drive end rotor for increasing static loads. Operation at 13 krpm

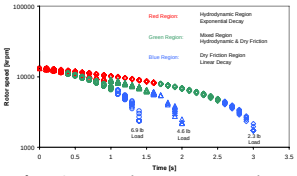

Fig. 10. Coastdown rotor speed versus time for increasing static loads. Data shows exponential (viscous) and linear (dry-friction) decay regions.

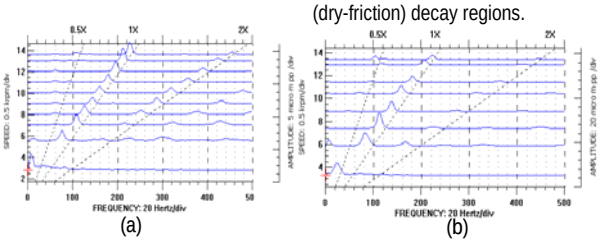

(a) (b)

Fig. 11. Rotor free end vibration cascade plots (a) with no applied load (b) 2 lb external load. Top rotor speed: 15.3 krpm. Super-synchronous rotor amplitudes (2X) decrease with applied load of 2lb.

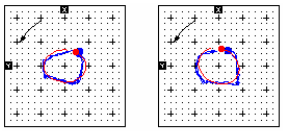

(a) 4,260 rpm (b) 7,770 rpm

(c) 11,800 rpm (d) 15,300 rpm

Fig. 12. Rotor free end orbits with no load at increasing shaft speeds: Blue: total motion orbit, Red: synchronous motion orbit. Largest orbit determines critical speed at ~ 7770 rpm

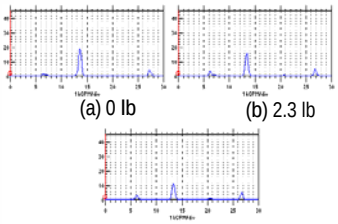

(a) 0 lb (b) 2.3 lb

(c) 4.6 lb

Fig. 13. Frequency spectrum of rotor free end, horizontal motions, at 15.3 krpm for (a) no external load (b) 2.3 lb load, and (c) 4.6 lb load. Note reduction in synchronous response as load magnitude increases.

Overall, test data show that increasing externally applied loads on rotor reduce the system rotordynamic response amplitudes of synchronous (1X) and (2X) frequencies. Foil bearings show increase in stiffness. Increasing static loads, however, produce shorter rotor coast down times, hence denoting larger dry-friction induced drag torque.

Acknowledgement

This study is supported by National Science Foundation under REU#0552885 program.